Macromolecules

pubs.acs.org/Macromolecules Article

Isotactic Poly(*ortho*-Fluorostyrene): Synthesis, Mechanism, and Intramolecular F−H Locking Promoted Crystallinity and Solvent Resistance

Qiyuan Wang, Hai Wang, Zhen Zhang, and Dongmei Cui*

Cite This: *Macromolecules* 2025, 58, 9402−9411 Read Online

ACCESS | Metrics & More | Article Recommendations | Supporting Information

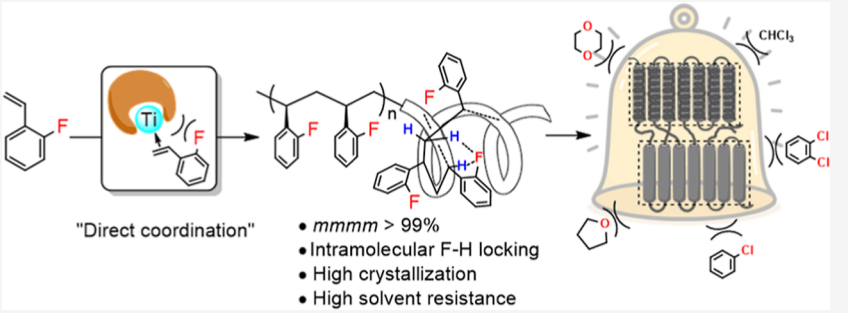

ABSTRACT: A highly isotactic poly(*ortho*-fluorostyrene) (*i*P*o*FS) was successfully synthesized via coordination polymerization using a 2,2′-sulfur-bridged bis(phenolato) titanium dichloro complex. The resultant *i*P*o*FS exhibited a melting point up to 261 °C with exceptional crystallinity and high hydrophobicity and solvent resistance as well as superior mechanical properties (tensile strength of 60.4 MPa) over commercial syndiotactic polystyrene (*s*PS) and all other polar groups substituted polystyrenes. Isospecific *o*FS and St copolymers revealed tunable crystallinity and thermal properties depending on *o*FS/St composition, which containing ≥50 mol % *o*FS content exhibit melting points exceeding that of *i*P*o*FS, although isotactic polystyrene (*i*PS) sequences have slow crystallization rate and low crystallinity. NMR, DSC, and XRD analyses confirmed the isotactic configuration and crystalline nature of these (co)polymers. DFT calculations indicated that the fluorine substituent of *o*FS does not participate directly in the polymerization process but stabilizes the 3_1 helical conformation of *i*P*o*FS through intramolecular F−H interaction, thereby contributing enhanced crystallization and remarkable resistance to organic solvents. These findings demonstrate that the steric bulky ligand is crucial to isospecific selectivity and to prevent polar group coordination, while the intramolecular superinteraction endows polymer materials with unprecedented physical and mechanical performances.

INTRODUCTION

Polystyrene is a cost-effective polymer material existing in three types of structure forms with distinct properties and applications. Atactic polystyrene (*a*PS), a general-purpose plastic, has been widely utilized as foaming and thermal insulation, etc., materials. Syndiotactic polystyrene (*s*PS), on the other hand, is an advanced engineering plastic, which exhibits high melting point, rapid crystallization rate, and excellent solvent resistance, rendering it high-end applications in the automotive and electronics industries.[1−5] In contrast, isotactic polystyrene (*i*PS) has not yet found any practical applications due to its significantly lower crystallization rate and inferior thermal stability compared to *s*PS, although it was originally synthesized upon the discovery of Ziegler−Natta or anionic catalysts.[6,7] Nevertheless, potential applications of *i*PS in specialized fields like optically active helical materials continually drive significant research efforts on enhancing *i*PS properties. Among various strategies, introducing polar functional groups to impart desirable characteristics including improved hydrophilicity, adhesion, dyeability, and compatibility with polar materials has proven to be the most direct and effective approach.[8] However, two major challenges hinder the development of highly isotactically functionalized polystyrene. First, there are few efficient catalysts capable of achieving high isoselectivity for styrene (St) polymerization as compared to those for *s*PS.[6,9−13] This limitation arises from the inherent conflict between the most sterically crowded coordination environment required for isoselective polymerization as compared to the syndioselective one and the open coordination environment demanding high catalytic activity, especially for bulky styrenyl monomers. Second, the strong

Received: June 17, 2025
Revised: August 13, 2025
Accepted: August 15, 2025
Published: August 22, 2025

https://doi.org/10.1021/acs.macromol.5c01607
Macromolecules 2025, 58, 9402−9411

Scheme 1. Stereoselective Polymerization of Polar Styrenes

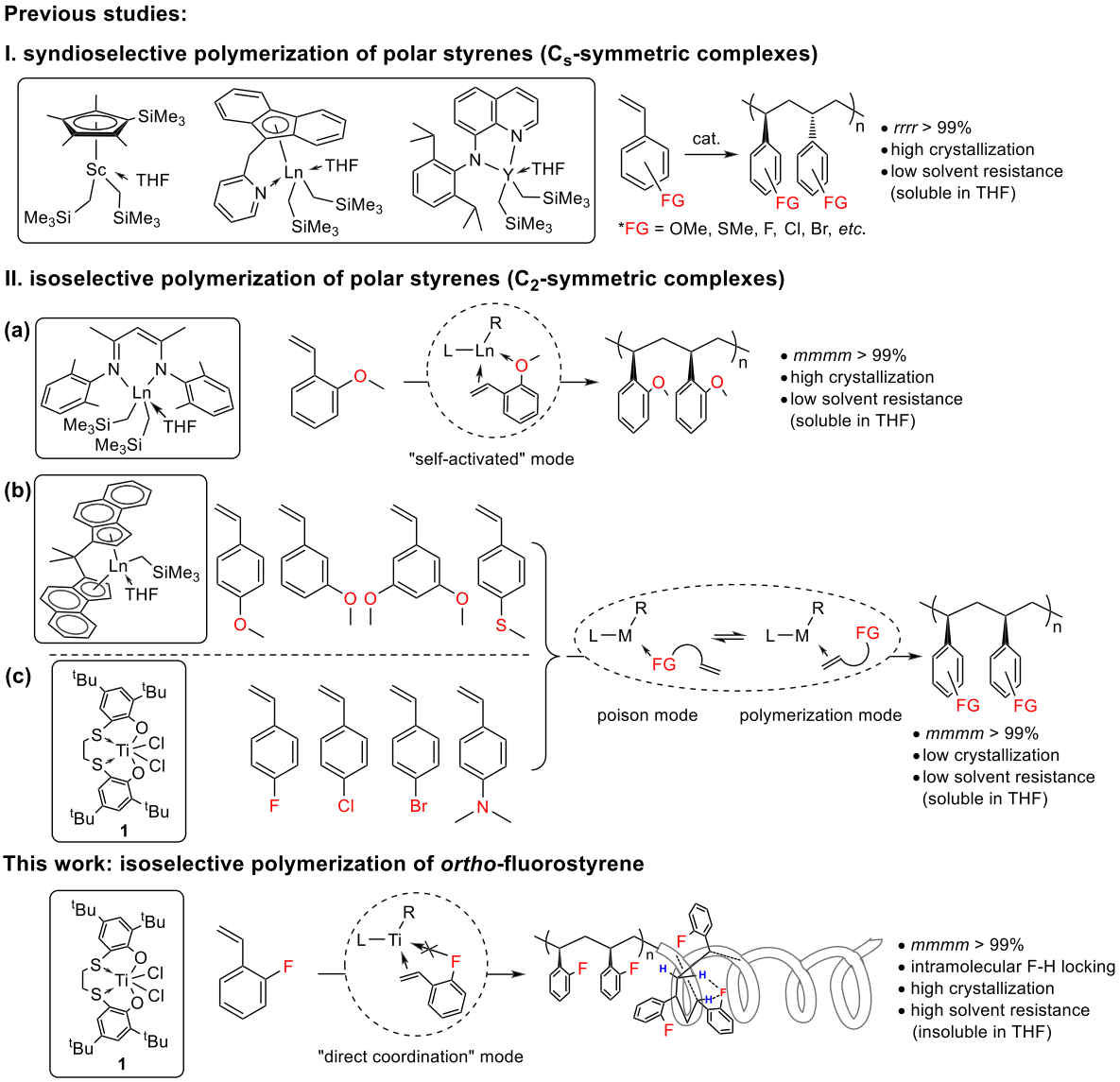

chelating effect of polar functional groups to the catalytic metal center usually leads to catalyst deactivation.[13−16] By means of the C_s-symmetric or side arm effect of catalysts, substantial progress has been made for the syndioselective polymerization of polar styrenes bearing methoxyl, methylthio, and even the electron-withdrawing halogenated styrene monomers despite of substituted positions of polar groups on the phenyl ring (Scheme 1, I).[17−34] Comparatively, research on isoselective polymerization by using a similar strategy has still stayed in place. A breakthrough was achieved in 2015 by developing a *β*-diketiminato rare-earth metal complex able to catalyze highly isoselective polymerization of *ortho*-methoxystyrene (*o*MOS) through the unprecedented "self-activated" mechanism. However, this system exhibited negligible activity toward other polar styrenes (Scheme 1, IIa).[16,35] More recently, in 2021, a series of rare-earth metal catalysts featuring racemic *ansa*-bis(benz[*e*]indenyl) ligands were reported to catalyze the highly isoselective polymerization of *para*-methoxystyrene (*p*MOS), *meta*-methoxystyrene (*m*MOS), 3,5-dimethoxystyrene (3,5-DMOS), and *para*-methylthiostyrene (*p*MTS), as well as the copolymerization with styrene (Scheme 1, IIb).[13]

Unfortunately, these catalysts remained inactive toward halogenated styrenes, although incorporation of halogen atoms is expected to enhance critical material properties such as thermal stability, corrosion resistance, chemical durability, etc.[36−39] The relatively small size fluorine allows more fluorostyrene (FSt) simultaneously coordinating to the metal center in F-*σ*-M mode to block the subsequent insertion and propagation.[22] Big and electron-withdrawing chlorine and bromine reduce electronic density of the reaction-double bonds to decrease activity of the substituted styrenes.[24] Obviously, achieving efficient polymerization of halogenated styrenes requires a highly Lewis acidic metal center and a suitably balanced steric environment. Therein, 2,2′-sulfur-bridged bis(phenolato)titanium dichloro complex **1** originally reported by Okuda and co-workers[11] might meet such criteria, which was employed by us to achieve the highly isotactic polymerization of *para*-fluorostyrene (*p*FS) (Scheme 1, IIc).[14] Note that neither isotactic poly(*para*-chlorostyrene) (*i*P*p*ClS) nor isotactic poly(*para*-bromostyrene) (*i*P*p*BrS) displays a detectable melting transition, only isotactic poly(*para*-fluorostyrene) (*i*P*p*FS) exhibited a relatively high melting

https://doi.org/10.1021/acs.macromol.5c01607
Macromolecules 2025, 58, 9402−9411

Table 1. Isoselective Homopolymerization of *o*FS with Complex 1[a]

Run	[*o*FS]/[Ti] (mol/mol)	time (h)	Temp. (°C)	Conv. (%)	Act. (10^4)[b]	M_n(10^4)[c]	M_w/M_n[c]	*mmmm*[d] (%)	T_g/T_m (°C)[e]	ΔH (J g^{-1})[e]
1	500/1	2	0	35	1.07	10.5	1.62	>99	77/261	41.5
2	500/1	2	25	62	1.90	17.7	1.64	>99	83/261	35.9
3	500/1	2	40	58	1.77	8.3	1.92	>99	84/261	38.8
4	500/1	2	60	55	1.68	4.9	1.77	>99	77/255	38.5
5	1000/1	5	25	82	2.00	19.0	1.58	>99	83/260	35.8
6	1500/1	7	25	86	2.25	25.2	1.64	>99	82/257	34.2
7	3000/1	12	25	87	2.66	32.9	1.72	>99	84/256	30.1

[a]General conditions: complex, 10 μmol; [Ti]/[Ph_3C][$B(C_6F_5)_4$]/Al^iBu_3 = 1/1/30 (mol/mol/mol); [*o*FS] = 3.125 mol/L in toluene solution. [b]Given in 10^4 g mol_{Ti}^{-1} h^{-1}. [c]Determined by GPC in 1,2,4-trichlorobenzene at 150 °C against polystyrene standard. [d]Determined by ^{1}H and ^{13}C NMR. [e]Determined by DSC.

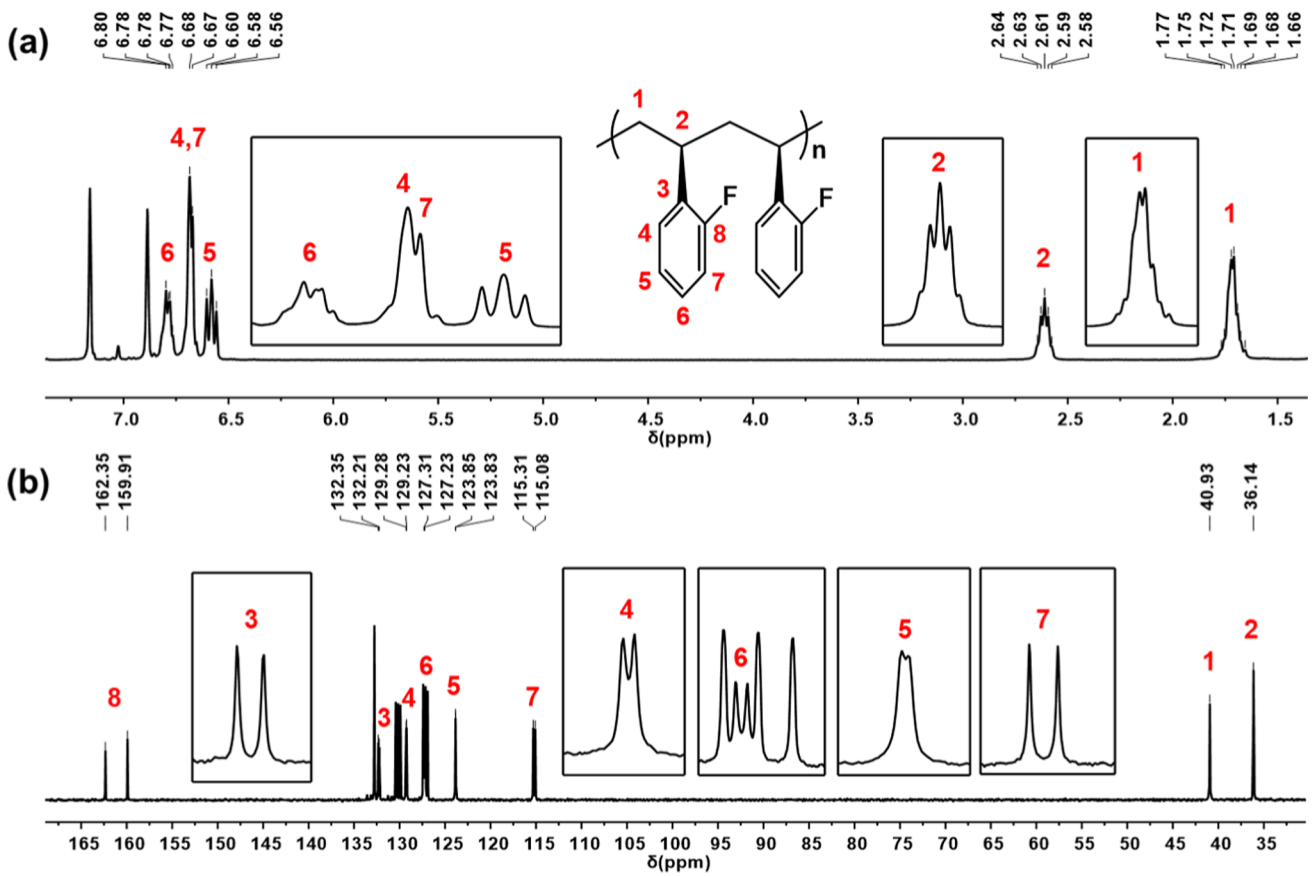

Figure 1. ^{1}H (a) and ^{13}C (b) NMR spectra of *i*P*o*FS ($C_6Cl_2D_4$, 110 °C) (Table 1, run 2).

point (234−253 °C). We hypothesized that the highly electronegative and weakly polarizable fluorine atom plays a unique role in promoting polymer crystallization. Keeping in mind that only isotactic poly(*ortho*-methoxystyrene) (*i*P*o*MOS) not isotactic poly(*meta*-methoxystyrene) (*i*P*m*MOS) or isotactic poly(*para*-methoxystyrene) (*i*P*p*MOS) exhibits a detectable melting point,[13,16] *ortho*-substituted polystyrenes and specific interactions between the substituents and the main chain may facilitate crystallization. Based on this knowledge, we are particularly interested in whether we can synthesize isotactic poly(*ortho*-fluorostyrene) (*i*P*o*FS) that has not been accessed yet and what properties *i*P*o*FS may possess.

In this study, we successfully synthesized highly *i*P*o*FS and its copolymers with styrene using a 2,2′-sulfur-bridged bis(phenolato) titanium dichloro complex **1**. Strikingly to us, *i*P*o*FS has a high melting point and a rapid crystallization rate. Its pronounced crystallinity endows the material with exceptional solvent resistance, exceeding all previously reported stereoregular polar polystyrenes as well as some conventional solvent-resistant polymers. Density functional theory (DFT) calculations further demonstrated that due to the unique coordination environment provided by the catalyst, the *ortho*-fluorine atom of *ortho*-fluorostyrene (*o*FS) does not chelate to the active metal center during coordination/insertion of the C═C bond. This minimizes catalyst deactivation to ensure efficient polymerization. Surprisingly, these fluorine substituents promote *i*P*o*FS strong crystallization ability through the intramolecular noncovalent interaction with δ-hydrogen atoms on the polymer main chain, which endows *i*P*o*FS with exceptional solvent resistance through stabilizing the 3_1 helical conformation.

https://doi.org/10.1021/acs.macromol.5c01607
Macromolecules 2025, 58, 9402−9411

Table 2. Isoselective Copolymerization of *o*FS with Complex 1[a]

run	[oFS]/[St]/[Ti] (mol/mol/mol)	time (h)	Conv. (%)	f_{oFS} (mol %)	$M_n(10^4)$[b]	M_w/M_n[b]	T_g/T_m (°C)[c]	ΔH (J g^{-1})[c]
1	50/450/1	12	100	10	15.5	1.53	93/236	3.4
2	150/350/1	12	100	30	11.5	1.54	85/252	24.7
3	250/250/1	12	100	50	16.1	1.61	88/263	28.3
4	350/150/1	12	100	70	13.2	1.50	90/269	37.6
5	450/50/1	12	100	90	11.5	1.42	84/266	34.2

[a]General conditions: complex, 10 μmol; [Ti]/[Ph_3C][$B(C_6F_5)_4$]/Al^{i}Bu$_3$ = 1/1/30 (mol/mol/mol); monomer = 3.125 mol/L in toluene solution. [b]Determined by GPC in 1,2,4-trichlorobenzene at 150 °C against polystyrene standard. [c]Determined by DSC.

RESULTS AND DISCUSSION

Homopolymerization of *o*FS. The polymerization of *o*FS was conducted using complex **1** in combination with [Ph_3C][$B(C_6F_5)_4$] and Al^{i}Bu$_3$ as the catalytic system, which had previously demonstrated isoselectivity for *p*FS.[14] The polymerization behavior of the catalyst was systematically investigated over a temperature range of 0 to 60 °C (Table 1, runs 1−4). At a low temperature of 0 °C, polymerization was significantly retarded to reach only 35% monomer conversion within 2 h. With increasing temperature, the catalytic activity increased to reach a maximum at 25 °C (1.90×10^4 g mol$_{Ti}^{-1}$ h^{-1}), which decreased slightly at higher temperatures. Notably, the increase of polymerization temperature resulted in a substantial drop of polymer molecular weight from 17.7×10^4 g mol^{-1} at 25 °C to 4.9×10^4 g mol^{-1} at 60 °C, which was primarily attributed to the enhanced initiation efficiency of the catalyst. At the optimal polymerization temperature of 25 °C, the effect of the monomer-to-catalyst feed ratio on the polymerization process was further examined (Table 1, runs 5−7). The results indicated that varying the ratio from 500:1 to 3000:1 led to a gradually enhanced molecular weight, reaching up to 32.9×10^4 g mol^{-1}, while the molecular weight distribution remained relatively stable (from 1.58 to 1.72). NMR spectroscopic analysis (Figures 1, S29−S34, and S40) confirmed that all polymers exhibited over *mmmm* >99% isotacticity by showing the quintet centered at δ 2.61 ppm and the multiplet at δ 1.71 ppm in the ^{1}H NMR spectrum, corresponding to the methine and asymmetric methylene protons, respectively (Figure 1a). The sharp singlets at δ 40.93 ppm (methylene carbon) and δ 36.14 ppm (methine carbon) in the ^{13}C NMR spectrum (Figure 1b) further substantiated the high isotacticity of the polymers. All fluorine-substituted phenyl carbon peaks appeared as doublets due to ^{19}F coupling, a phenomenon commonly observed in the stereoregular poly(FSt)s.[14,22,25] Additionally, it also exhibits a sharp single peak in the ^{19}F NMR spectrum (Figure S40). The resulting polymers exhibited high melting temperatures in the range of 255−261 °C with melting enthalpies of 30.1 to 41.5 J g^{-1}. These values significantly exceeded those of syndiotactic poly(*ortho*-fluorostyrene) (*s*P*o*FS) (T_m = 245 °C, ΔH = 21 J g^{-1}) and *i*P*p*FS (T_m = 234−253 °C, ΔH = 0.32−23.2 J g^{-1}),[14,25] indicating substantially enhanced crystallization rates and crystallinities.

Copolymerization of *o*FS and St. The melting point of *i*P*o*FS is significantly higher than that of its syndiotactic counterpart, in contrast to the trend observed in nonpolar polystyrenes, where *s*PS exhibits a higher melting point than *i*PS. This behavior suggests that the chain segments in *i*P*o*FS strongly promote crystallization. To further investigate this crystallization phenomenon, we conducted a copolymerization of *o*FS with St, thereby incorporating *i*PS, which possesses an inherently weak crystallization ability, into the *i*P*o*FS matrix. In these reactions, the total monomer-to-catalyst ratio was fixed at 500:1, while the molar ratio of *o*FS to St was varied stepwise. All polymerizations reached complete conversion within 12 h, yielding copolymers with *o*FS contents ranging from 10 to 90 mol % (Table 2). The resulting copolymers exhibited number-average molecular weights in the range of 11.5−16.1 × 10^4 g mol^{-1} with narrow molecular weight distributions (M_w/M_n = 1.42−1.61). Remarkably, the melting points of the copolymers containing 50, 70, and 90 mol % *o*FS (T_m = 263−269 °C) exceeded 261 °C of *i*P*o*FS (Figure 2). Moreover, all

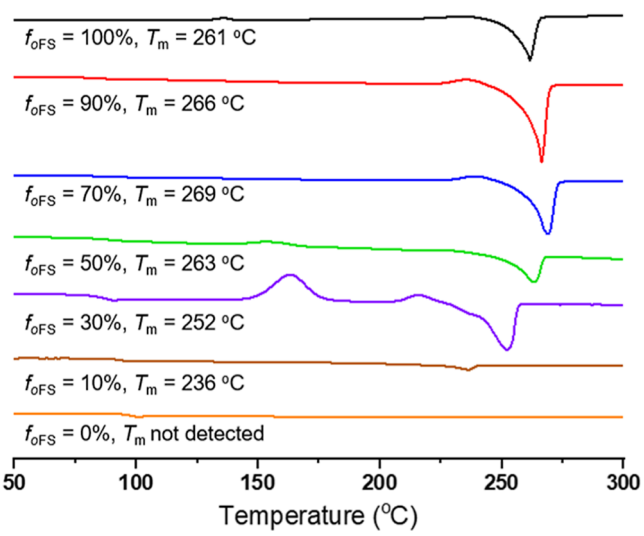

Figure 2. DSC curves of *o*FS-St copolymers with different *o*FS contents (f_{oFS} = 0−100%).

copolymers except the one containing 10 mol % *o*FS exhibited high melting enthalpies (ΔH = 24.7−37.6 J g^{-1}), further confirming their excellent cocrystallization performance. To the best of our knowledge, this represents the first report about a copolymer which gives a higher melting point after incorporating a component reluctant to crystallize.[21−25,31,34]

To further investigate the sequence distribution within the copolymer, copolymerization kinetics was studied at low monomer conversions (below 5%). Based on the Fineman−Ross equation, the monomer reactivity ratios were determined to be r_{oFS} = 0.501 and r_{St} = 1.604 (Table S1 and Figure 3), indicating a random sequence distribution of *o*FS and St units along the polymer chain. Structural insights into the copolymer were obtained from a detailed analysis of the ^{13}C NMR spectrum (Figure 4). Signals in the range of δ 146.7−146.4, 146.2−145.9, and 145.8−145.5 ppm correspond to the *ipso* carbons of styrene units in the SSS, SSF, and FSF triads, respectively (where S denotes a styrene unit and F denotes an *o*FS unit). Similarly, peaks at δ 133.2−132.8, 132.7−132.3, and 132.3−131.9 ppm represent the *ipso* carbons of *o*FS units in

https://doi.org/10.1021/acs.macromol.5c01607
Macromolecules 2025, 58, 9402−9411

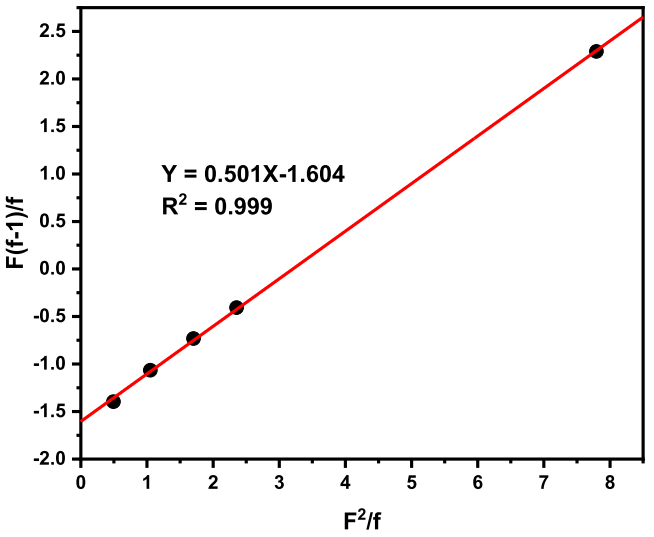

Figure 3. Fineman–Ross plot for the copolymerization of *o*FS and St and least-squares best fit line.

the SFS, SFF, and FFF triads, respectively. These results further confirmed a random incorporation of both monomers with the relative abundance of various triad structures varying systematically with the monomer feed ratio. In the copolymer containing 10 mol % *o*FS, *o*FS units are predominantly isolated along the polymer backbone (Figure 4a). When the *o*FS content is increased to 30 mol %, approximately half of the *o*FS units exist as adjacent pairs (Figure 4b). At higher *o*FS contents, distinct consecutive *o*FS units emerge to form longer isotactic segments (Figure 4c–e). In the ^{19}F NMR spectrum (Figure S41), the variation pattern of F atoms in copolymers with different *o*FS contents is consistent with that observed in the ^{13}C NMR spectrum. Correlating these observations with DSC results, it can be concluded that isolated *o*FS units contribute minimally to crystallization. Effective promotion of crystallization requires at least paired *o*FS units, and long consecutive *o*FS sequences result in a significantly enhanced crystallinity.

X-ray Diffraction Analysis. To elucidate the origin of high melting points observed in polymers, we used *o*FS content of 100% (*o*FS100), 70% (*o*FS7030), and 50% (*o*FS5050), respectively. X-ray diffraction analysis was performed. Each polymer sample was examined under two conditions—before and after thermal annealing—to assess differences in the crystallinity (Figure 5). The annealing temperatures were

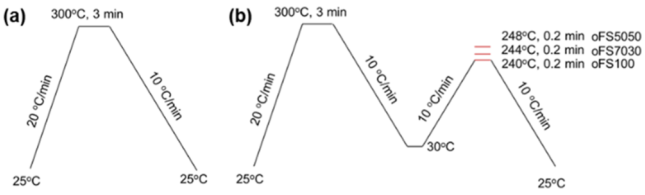

Figure 5. (a) Heating–cooling DSC program and (b) annealing DSC program for sample treatment.

selected based on the corresponding DSC data (Figure S28), specifically near the end of the crystallization exotherm and the onset of melting, which occurred at 240 °C, 244 °C, and 248 °C for the respective polymers.

As shown in Figure 6, the nearly overlapping 1D-WAXD profiles indicate that the crystallinity (X_c) values of the three samples are rather close. The 1D-SAXS curves show the peak value corresponding to very close q value, which can be indicated using $I(q)q^2$ vs q curves below. According to Bragg's law ($q = 2\pi/d_{ac}$), this indicates that the polymers possess comparable long periods (d_{ac}). Based on the relationship $d_{ac}\cdot X_c = d_c$, where d_c is the lamellar thickness, it can be inferred that the three samples subjected to the heating–cooling program exhibit nearly identical d_c. Figure 7 shows the 1D-WAXD and 1D-SAXS curves from the annealing program. It seems there is no profound difference in crystallinity from 1D-WAXD profiles or long period from 1D-SAXS. The d_c seems to have no obvious difference. These results indicate that polymers with

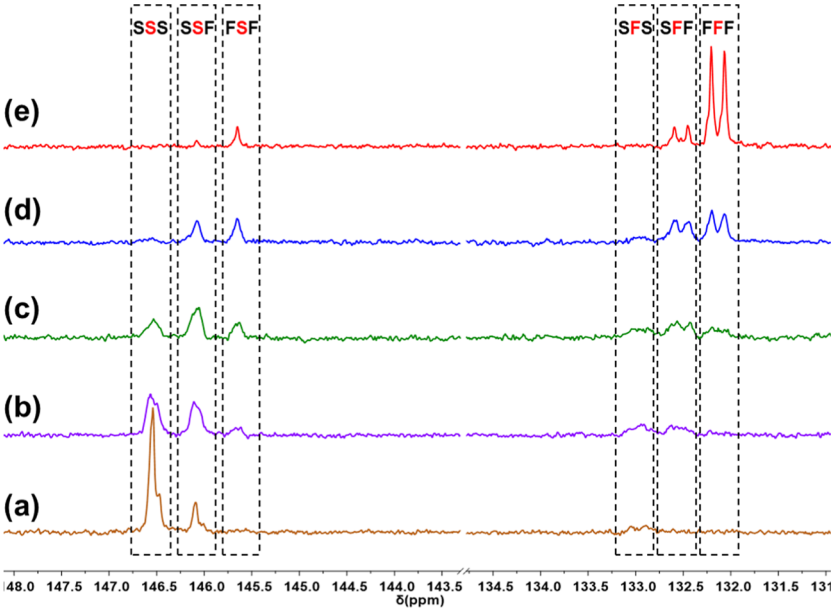

Figure 4. ^{13}C NMR spectra of isotactic poly(*o*FS-*co*-St) ($C_2D_2Cl_4$, 110 °C) (Table 2, runs 1–5): (a) f_{oFS} = 10 mol %; (b) f_{oFS} = 30 mol %; (c) f_{oFS} = 50 mol %; (d) f_{oFS} = 70 mol %; (e) f_{oFS} = 90 mol %.

https://doi.org/10.1021/acs.macromol.5c01607
Macromolecules 2025, 58, 9402–9411

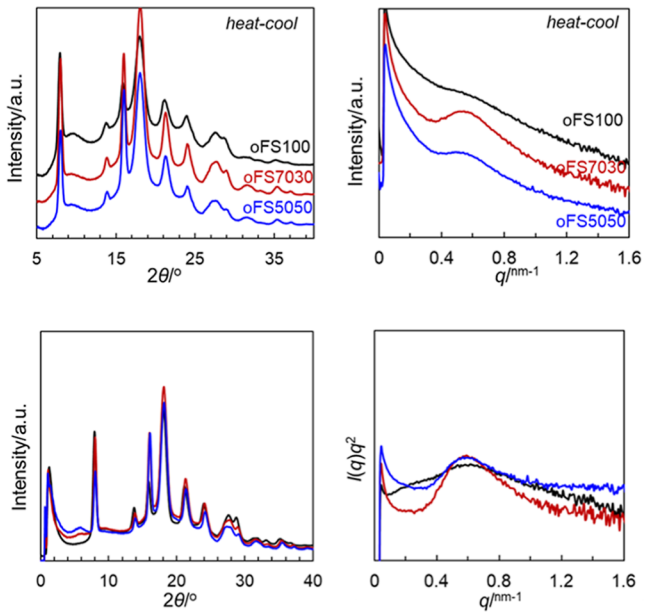

Figure 6. 1D-WAXD and 1D-SAXS profiles of samples *o*FS100, *o*FS7030, and *o*FS5050 treated by heating−cooling program.

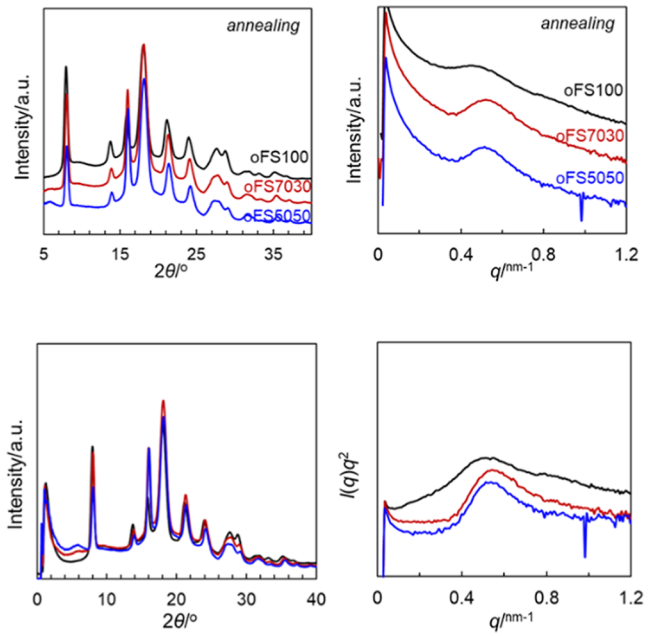

Figure 7. 1D-WAXD and 1D-SAXS profiles of samples oFS100, oFS7030, and oFS5050 treated by annealing program.

*o*FS contents of 100%, 70%, and 50% exhibit comparable levels of crystallinity and lamellar thickness, which accounts for their similarly high melting points.

The pronounced crystallinity of *i*P*o*FS substantially enhances its mechanical properties, exhibiting a tensile strength of 60.4 MPa and an elongation at break of 4.0% (Figure S1), outperforming commercial *s*PS[40] showing a tensile strength of 47.0 MPa and an elongation at break of 2.3%. As the *o*FS content in the copolymer decreases, a corresponding decline in the mechanical properties is observed. This reduction is attributed to the incorporation of *i*PS segments, which possess lower crystallinity and thus negatively impact the overall performance of the copolymer.

Solvent Resistance. The solubility of crystalline polymers in solvents is closely related to the stability of their crystalline domains. All previously reported stereoregular polar polystyrenes are soluble in tetrahydrofuran (THF) at room temperature, indicating limited crystalline stability and susceptibility to solvent penetration to facilitate dissolution. The obtained *i*P*o*FS experienced extensive-solubility tests (Table S2) to exhibit exceptional solvent resistance toward the most common solvents including THF. Complete dissolution only happened when their *o*-dichlorobenzene solutions were heated to 180 °C, surpassing the thermal dissolution thresholds of conventional solvent-resistant polymers such as *s*PS, ultrahigh molecular weight polyethylene (UHMWPE), and isotactic polypropylene (*i*PP), which typically dissolve under temperatures below 160 °C (Table S3). For comparison, *s*P*o*FS and *i*P*p*FS revealed significantly lower solvent resistance to readily dissolve in the most common solvents at comparatively lower temperatures (Table S2). Moreover, solutions of *s*P*o*FS and *i*P*p*FS remained transparent and stable for at least 48 h upon cooling to room temperature without any sign of precipitation. In contrast, *i*P*o*FS solutions formed flocculent precipitates within 12 h due to potential self-assembly behavior (Figure 8). Solubility tests

Figure 8. State of the polymer solution (in *o*-dichlorobenzene) after (a) heating and (b) cooling to room temperature for 12 h.

were also conducted on isotactic *o*FS-St copolymers (Table S4). The dissolution temperature of the copolymers was dependent on the *o*FS content. With the *o*FS molar fraction increasing, the dissolution temperature increases progressively from 100 °C for *o*FS1090 to 130 °C for *o*FS3070 and further to 160 °C for *o*FS5050. Notably, copolymers containing ≥70 mol % *o*FS precipitated from the cooled solution at room temperature (Figure 8), further indicating a link between *o*FS content and solvent resistance.

Both *i*P*o*FS and *i*PS crystals adopt a 3_1 helical conformation,[41−43] which was investigated via DFT simulation by using a short polymer segment model (Figure 9). Natural Bond Orbital (NBO) analysis revealed that the fluorine atoms in *i*P*o*FS engage in noncovalent interactions with both α-H on the main chain and δ-H on the same side of the helix. Particularly, the interaction between the fluorine atom and δ-H facilitates the formation of the helical structure and its

https://doi.org/10.1021/acs.macromol.5c01607
Macromolecules 2025, 58, 9402−9411

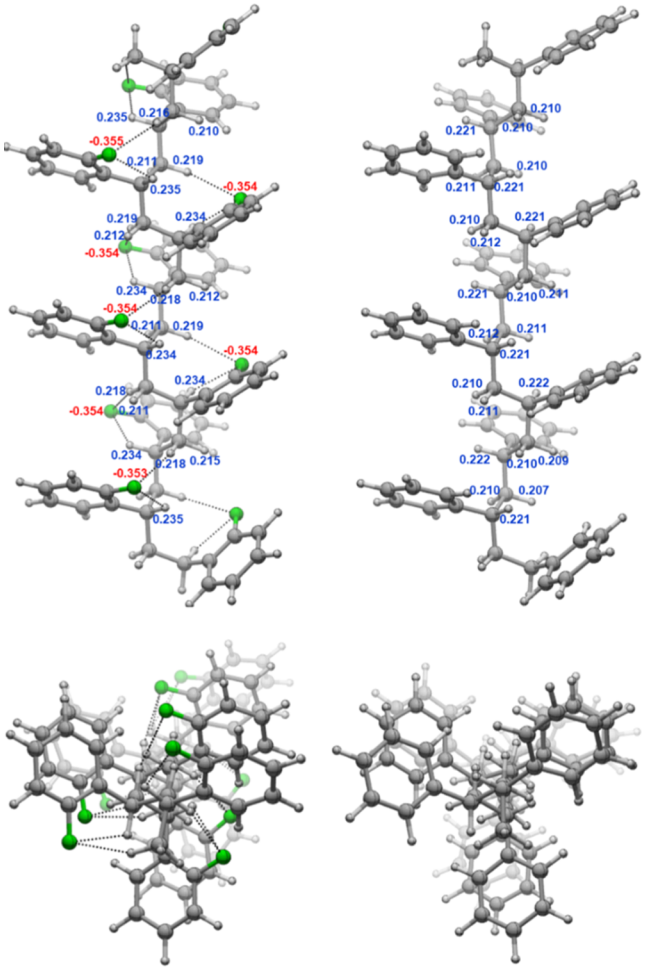

Figure 9. Optimized structures of *i*P*o*FS and *i*PS (side and end views).

stabilization. On the contrary, such interactions are absent in *i*PS. Therefore, the stable and rigid helical structure is conducive to the enhanced crystallinity of *i*P*o*FS and its distinguished solvent resistance. It is expected that *i*P*o*FS contains irregular amorphous regions in which the orientation of the fluorine atoms is disordered. We further simulated two scenarios (Figure S2): model I with all fluorine atoms being oriented in the opposite direction and model II with all fluorine atoms alternatingly arranging in two directions. In model I, each F atom interacts with only two adjacent β-hydrogen atoms. This conformation provides limited stabilization for the helical structure and exhibits a total energy 2.3 kcal/mol higher than that of the original structure. In model II, approximately half of the F atoms still contribute to helical stabilization, and the overall energy is only 0.3 kcal/mol higher than that of the original structure. However, in model II, there are regions (highlighted with red circles) where F atoms cannot exert effective conformational control. In these areas, C−C bonds are more likely to rotate, disrupting the helical configuration. These structures may indeed exist in the polymer, but they are intrinsically less stable. Additionally, unlike conventional polar polymers, *i*P*o*FS demonstrates characteristic features of low surface energy and pronounced hydrophobicity[44−46] by displaying a low water contact angle varying from 106.8° for *o*FS100 to the lowest 96.9° for *o*FS1090 approaching to 94° for the nonpolar *i*PS (Figure S3).

Polymerization Mechanism. In the coordination polymerization of polar monomers, polar groups typically exhibit a strong tendency to coordinate with the metal center. Depending on the monomer configuration, two coordination modes can occur: (1) a "self-activated" mode, in which both the polar group and the double bond simultaneously coordinate to the metal center, or (2) a "skip coordination" mode, involving a transition from the polar-group coordination to the double-bond coordination. In scenario (2), the energy required for dissociation of the polar group often exceeds the energy gained from recoordination of the double bond, resulting in an overall increase of system energy. In this system, *o*FS exists in two geometric configurations: *syn* and *anti*. DFT simulations reveal that $o\mathrm{FS}_{\mathrm{syn}}$ (1.48 kcal mol^{-1}) is energetically less stable than $o\mathrm{FS}_{\mathrm{anti}}$ (0 kcal mol^{-1}) (Figure S4). Based on the Boltzmann statistics equation,[47] the concentration of $o\mathrm{FS}_{\mathrm{anti}}$ is 12.2 times higher than that of $o\mathrm{FS}_{\mathrm{syn}}$, making $o\mathrm{FS}_{\mathrm{anti}}$ the dominant species, and thus, it is selected for further investigation. During the initiation stage, attempts to locate the σ-π coordinate mode involving both fluorine and the double bond were unsuccessful. Considering that the *anti*-configuration introduces greater steric hindrance, $o\mathrm{FS}_{\mathrm{syn}}$ was also examined; however, a similar coordination location failed due to the great steric hindrance around the metal center (Figure S5). Therefore, we simulated the transition from F−σ−Ti coordination skipping to C═C−η^2−Ti coordination. Interestingly, coordination of the double bond yielded a more stable complex than coordination via the fluorine atom (Figure 10), suggesting that C═C−η^2−Ti coordination is energetically favored (C1−F vs C1)—an unusual phenomenon in polar monomer polymerization. This preference was also confirmed for $o\mathrm{FS}_{\mathrm{syn}}$ (Figure S6). For chain initiation, $o\mathrm{FS}_{\mathrm{anti}}$ exhibits the lowest activation energy via the transition state of $\mathbf{TS1}_{\mathrm{re21}}$ (9.0 kcal mol^{-1}) and the most stable intermediate $\mathbf{P1}_{\mathrm{re21}}$ (−14.8 kcal mol^{-1}), for 2,1-insertion on the *re*-face. This pathway is favored due to the reduced steric repulsion among the monomer, ligand, and initiator group as compared to other coordination modes (Figure S7). Simulations for St polymerization involve a 2,1-insertion on the *re*-face with a slightly lower activation energy (8.4 kcal mol^{-1}) and a more stable intermediate (−15.5 kcal mol^{-1}) than $o\mathrm{FS}_{\mathrm{anti}}$ (Figure S8), which is consistent with experimental observations of slightly higher activity for St polymerization. During the insertion of the second and third $o\mathrm{FS}_{\mathrm{anti}}$, the *C*2-symmetry of the complex favors consecutive 2,1-insertion on the *re*-face (Figure 10), leading to the formation of fully i*P*o*FS*.

■ CONCLUSIONS

In summary, we have successfully achieved the highly isoselective coordination polymerization of *o*FS with the 2,2′-sulfur-bridged bis(phenolato) titanium dichloro complex. Mechanism investigation reveals that the isoselectivity is caused mainly by the sterically bulky coordination environment of the catalyst, since the commonly occurring η^2-C═C: σ−F−Ti chelation between the *ortho*-fluoro atom and C═C with the Ti metal center is absent. However, the strong intramolecular noncovalent interactions between fluorine atoms and hydrogen atoms on the polymer backbone are essential for the exceptional physical and mechanical, especially distinguished solvent-resistance properties of *i*P*o*FS. The interactions prompt crystallinity for both *i*P*o*FS and its copolymer with *i*PS that is reluctant to crystallize, which also facilitate formation of the 3_1 helical structure of *i*P*o*FS as

https://doi.org/10.1021/acs.macromol.5c01607
Macromolecules 2025, 58, 9402−9411

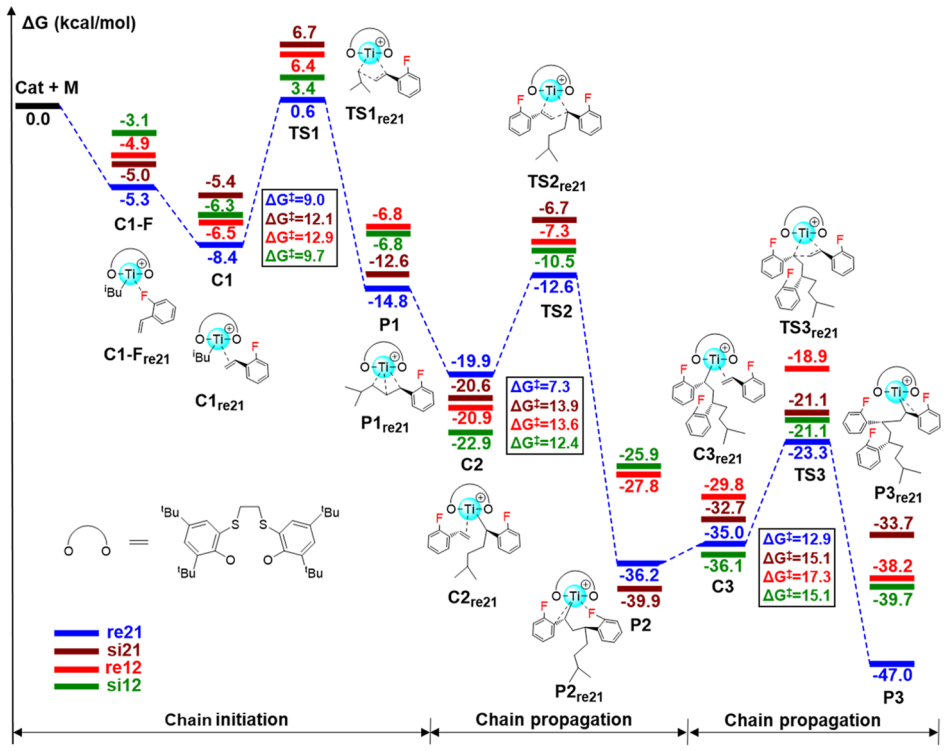

Figure 10. Energy profiles for the polymerization of *o*FS$_{anti}$.

confirmed by DFT calculations. This study underscores potential applications of *i*P*o*FS as a high-performance fluorinated polymer where enhanced crystallization behavior is critical, such as nucleating agents, self-assembling systems, and structural materials of antisolvent under high temperatures.

■ ASSOCIATED CONTENT

Supporting Information

The Supporting Information is available free of charge at https://pubs.acs.org/doi/10.1021/acs.macromol.5c01607.

Detailed experimental procedures, copolymerization data, solubility comparison of polymers, stress−strain curves for polymers, water contact angle of polymers, DFT calculations, GPC data, DSC data, and NMR spectra of polymers (PDF)

■ AUTHOR INFORMATION

Corresponding Author

Dongmei Cui − *State Key Laboratory of Polymer Physics and Chemistry, Changchun Institute of Applied Chemistry, Chinese Academy of Sciences, Changchun 130022, China; School of Applied Chemistry and Engineering, University of Science and Technology of China, Hefei 230026, China;* orcid.org/0000-0001-8372-5987; Email: dmcui@ciac.ac.cn

Authors

Qiyuan Wang − *State Key Laboratory of Polymer Physics and Chemistry, Changchun Institute of Applied Chemistry, Chinese Academy of Sciences, Changchun 130022, China; School of Applied Chemistry and Engineering, University of Science and Technology of China, Hefei 230026, China*

Hai Wang − *PetroChina (Shanghai) Advanced Materials Research Institute Co. Ltd., Shanghai 201306, China;* orcid.org/0000-0001-8902-4014

Zhen Zhang − *State Key Laboratory of Polymer Physics and Chemistry, Changchun Institute of Applied Chemistry, Chinese Academy of Sciences, Changchun 130022, China*

Complete contact information is available at: https://pubs.acs.org/10.1021/acs.macromol.5c01607

Author Contributions

The manuscript was written through contributions of all authors. All authors have given approval to the final version of the manuscript.

Notes

The authors declare no competing financial interest.

■ ACKNOWLEDGMENTS

This work was partially supported by the NSFC (project Nos. 22331010, U21A20279).

■ REFERENCES

(1) Tomotsu, N.; Ishihara, N.; Newman, T. H.; Malanga, M. T. Syndiospecific polymerization of styrene. *J. Mol. Catal. A: Chem.* **1998**, *128* (1), 167−190.

(2) Malanga, M. Syndiotactic Polystyrene Materials. *Adv. Mater.* **2000**, *12* (23), 1869−1872.

(3) Schellenberg, J.; Leder, H.-J. Syndiotactic polystyrene: Process and applications. *Adv. Polym. Technol.* **2006**, *25* (3), 141−151.

(4) Ishihara, N.; Seimiya, T.; Kuramoto, M.; Uoi, M. Crystalline syndiotactic polystyrene. *Macromolecules* **1986**, *19* (9), 2464−2465.

(5) Ishihara, N.; Kuramoto, M.; Uoi, M. Stereospecific polymerization of styrene giving the syndiotactic polymer. *Macromolecules* **1988**, *21* (12), 3356−3360.

(6) Natta, G.; Pino, P.; Corradini, P.; Danusso, F.; Mantica, E.; Mazzanti, G.; Moraglio, G. CRYSTALLINE HIGH POLYMERS OF α-OLEFINS. *J. Am. Chem. Soc.* **1955**, *77* (6), 1708−1710.
(7) Maréchal, J.-M.; Carlotti, S.; Shcheglova, L.; Deffieux, A. Stereospecific anionic polymerization of styrene initiated by R2Mg/ROMt 'ate' complexes. *Polymer* **2004**, *45* (14), 4641−4646.
(8) Tan, C.; Si, G.; Zou, C.; Chen, C. Functional Polyolefins and Composites. *Angew. Chem., Int. Ed.* **2025**, *64* (12), No. e202424529.
(9) Rodrigues, A.-S.; Kirillov, E.; Carpentier, J.-F. Group 3 and 4 single-site catalysts for stereospecific polymerization of styrene. *Coord. Chem. Rev.* **2008**, *252* (18), 2115−2136.
(10) Rodrigues, A.-S.; Kirillov, E.; Roisnel, T.; Razavi, A.; Vuillemin, B.; Carpentier, J.-F. Highly Isospecific Styrene Polymerization Catalyzed by Single-Component Bridged Bis(indenyl) Allyl Yttrium and Neodymium Complexes. *Angew. Chem., Int. Ed.* **2007**, *46* (38), 7240−7243.
(11) Capacchione, C.; Proto, A.; Ebeling, H.; Mülhaupt, R.; Möller, K.; Spaniol, T. P.; Okuda, J. Ancillary Ligand Effect on Single-Site Styrene Polymerization: Isospecificity of Group 4 Metal Bis-(phenolate) Catalysts. *J. Am. Chem. Soc.* **2003**, *125* (17), 4964−4965.
(12) Annunziata, L.; Rodrigues, A.-S.; Kirillov, E.; Sarazin, Y.; Okuda, J.; Perrin, L.; Maron, L.; Carpentier, J.-F. Isoselective Styrene Polymerization Catalyzed by ansa-Bis(indenyl) Allyl Rare Earth Complexes. Stereochemical and Mechanistic Aspects. *Macromolecules* **2011**, *44* (9), 3312−3322.
(13) Jiang, Y.; Zhang, Z.; Li, S.; Cui, D. Isospecific (Co)-polymerization of Unmasked Polar Styrenes by Neutral Rare-Earth Metal Catalysts. *Angew. Chem., Int. Ed.* **2022**, *134* (9), No. e202112966.
(14) Wang, Q.; Zhang, Z.; Jiang, Y.; Zhang, Y.; Li, S.; Cui, D. Isospecific Polymerization of Halide- and Amino-Substituted Styrenes Using a Bis(phenolate) Titanium Catalyst Catalysts. *Catalysts* **2022**, *12*, 439.
(15) De Carlo, F.; Capacchione, C.; Schiavo, V.; Proto, A. Reactivity of styrene and substituted styrenes in the presence of a homogeneous isospecific titanium catalyst. *J. Polym. Sci., Part A: Polym. Chem.* **2006**, *44* (4), 1486−1491.
(16) Liu, D.; Yao, C.; Wang, R.; Wang, M.; Wang, Z.; Wu, C.; Lin, F.; Li, S.; Wan, X.; Cui, D. Highly Isoselective Coordination Polymerization of ortho-Methoxystyrene with β-Diketiminato Rare-Earth-Metal Precursors. *Angew. Chem., Int. Ed.* **2015**, *54* (17), 5205−5209.
(17) Huang, J.; Liu, Z.; Cui, D.; Liu, X. Precisely Controlled Polymerization of Styrene and Conjugated Dienes by Group 3 Single-Site Catalysts. *ChemCatChem* **2018**, *10* (1), 42−61.
(18) Liu, D.; Wang, M.; Chai, Y.; Wan, X.; Cui, D. Self-Activated Coordination Polymerization of Alkoxystyrenes by a Yttrium Precursor: Stereocontrol and Mechanism. *ACS Catal.* **2019**, *9* (3), 2618−2625.
(19) Zhang, Z.; Jiang, Y.; Zhang, K.; Cai, Z.-Y.; Li, S.-H.; Cui, D.-M. DMAO-activated Rare-earth Metal Catalysts for Styrene and Its Derivative Polymerization. *Chin. J. Polym. Sci.* **2021**, *39* (9), 1185−1190.
(20) Liu, D.; Wang, R.; Wang, M.; Wu, C.; Wang, Z.; Yao, C.; Liu, B.; Wan, X.; Cui, D. Syndioselective coordination polymerization of unmasked polar methoxystyrenes using a pyridenylmethylene fluorenyl yttrium precursor. *Chem. Commun.* **2015**, *51* (22), 4685−4688.
(21) Guo, F.; Jiao, N.; Jiang, L.; Li, Y.; Hou, Z. Scandium-Catalyzed Syndiospecific Polymerization of Halide-Substituted Styrenes and Their Copolymerization with Styrene. *Macromolecules* **2017**, *50* (21), 8398−8405.
(22) Wang, Z.; Wang, M.; Liu, J.; Liu, D.; Cui, D. Rapid Syndiospecific (Co)Polymerization of Fluorostyrene with High Monomer Conversion. *Chem. Eur. J.* **2017**, *23* (72), 18151−18155.
(23) Zhong, Y.; Wu, Y.; Cui, D. Highly Syndiotactic Coordination (Co)polymerization of para-Methylselenostyrene. *Macromolecules* **2021**, *54* (4), 1754−1759.
(24) Wu, Y.; Wang, Z.; Liu, D.; Liu, B.; Cui, D. Highly Syndioselective Coordination (Co)Polymerization of para-Chlorostyrene. *Macromolecules* **2020**, *53* (19), 8333−8339.
(25) Wang, T.; Liu, D.; Cui, D. Highly Syndioselective Coordination (Co)Polymerization of ortho-Fluorostyrene. *Macromolecules* **2019**, *52* (24), 9555−9560.
(26) Xu, S.; Wang, J.; Zhai, J.; Wang, F.; Pan, L.; Shi, X. Imidazoline-2-imine Functionalized Fluorenyl Rare-Earth Metal Complexes: Synthesis and Their Application in the Polymerization of ortho-Methoxystyrene. *Organometallics* **2021**, *40* (19), 3323−3330.
(27) Song, C.; Chen, J.; Fu, Z.; Yan, L.; Gao, F.; Cao, Q.; Li, H.; Yan, X.; Chen, S.; Zhang, S.; Li, X. Syndiospecific Polymerization of o-Methoxystyrene and Its Silyloxy or Fluorine-Substituted Derivatives by HNC-Ligated Scandium Catalysts: Synthesis of Ultrahigh-Molecular-Weight Functionalized Polymers. *Macromolecules* **2021**, *54* (23), 10838−10849.
(28) Wang, R.; Liu, D.; Li, X.; Zhang, J.; Cui, D.; Wan, X. Synthesis and Stereospecific Polymerization of a Novel Bulky Styrene Derivative. *Macromolecules* **2016**, *49* (7), 2502−2510.
(29) Li, X.; Wang, R.; Wu, C.; Chen, J.; Zhang, J.; Cui, D.; Wan, X. Effect of the tactic structure on the chiroptical properties of helical vinylbiphenyl polymers. *Polym. Chem.* **2019**, *10* (28), 3887−3894.
(30) Shi, X.; Nishiura, M.; Hou, Z. Simultaneous Chain-Growth and Step-Growth Polymerization of Methoxystyrenes by Rare-Earth Catalysts. *Angew. Chem., Int. Ed.* **2016**, *55* (47), 14812−14817.
(31) Mu, X.; Li, Y. Syndiospecific coordination (Co)polymerization of carbazole-substituted styrene derivatives using the scandium catalyst system. *Polym. Chem.* **2021**, *12* (43), 6291−6299.
(32) Jiang, L.; Guo, F.; Shi, Z.; Li, Y.; Hou, Z. Syndiotactic Poly(aminostyrene)-Supported Palladium Catalyst for Ketone Methylation with Methanol. *ChemCatChem* **2017**, *9* (20), 3827−3832.
(33) Shi, Z.; Guo, F.; Li, Y.; Hou, Z. Synthesis of amino-containing syndiotactic polystyrene as efficient polymer support for palladium nanoparticles. *J. Polym. Sci., Part A: Polym. Chem.* **2015**, *53* (1), 5−9.
(34) Liu, D.; Wang, M.; Wang, Z.; Wu, C.; Pan, Y.; Cui, D. Stereoselective Copolymerization of Unprotected Polar and Nonpolar Styrenes by an Yttrium Precursor: Control of Polar-Group Distribution and Mechanism. *Angew. Chem., Int. Ed.* **2017**, *56* (10), 2714−2719.
(35) Chai, Y.; Wang, L.; Liu, D.; Wang, Z.; Run, M.; Cui, D. Polar-Group Activated Isospecific Coordination Polymerization of ortho-Methoxystyrene: Effects of Central Metals and Ligands. *Chem. Eur. J.* **2019**, *25* (8), 2043−2050.
(36) McNeill, I. C.; Ćoşkun, M. Structure and stability of halogenated polymers: Part 4 Chain brominated polystyrene. *Polym. Degrad. Stab.* **1989**, *25* (1), 1−9.
(37) Kawaguchi, H.; Sumida, Y.; Muggee, J.; Vogl, O. Head-to-head polymers: 19. Chlorination of cis-1,4-polybutadiene. *Polymer* **1982**, *23* (12), 1805−1814.
(38) Wiacek, M.; Jurczyk, S.; Kurcok, M.; Janeczek, H.; Schab-Balcerzak, E. Synthesis of polystyrene modified with fluorine atoms: Monomer reactivity ratios and thermal behavior. *Polym. Eng. Sci.* **2014**, *54* (5), 1170−1181.
(39) Sessions, L. B.; Cohen, B. R.; Grubbs, R. B. Alkyne-Functional Polymers through Sonogashira Coupling to Poly(4-bromostyrene). *Macromolecules* **2007**, *40* (6), 1926−1933.
(40) Wang, Q.; Zhang, Z.; Jiang, Y.; Li, S.; Cui, D. Synthesis of Ethylene−Styrene Multiblock Copolymers Possessing High Strength and Toughness Using Binuclear Scandium Catalysts. *Macromolecules* **2025**, *58* (5), 2609−2618.
(41) Natta, G.; Corradini, P.; Bassi, I. W. Crystal Structure of Poly-orthc-Fluorostyrene. *Nuovo Cim* **1960**, *15* (1), 83−95.
(42) Natta, G.; Corradini, P.; Bassi, I. W. Crystal structure of isotactic polystyrene. *Nuovo Cim* **1960**, *15* (1), 68−82.
(43) Natta, G.; Danusso, F.; Sianesi, D. Stereospecific polymerization and isotactic polymers of vinyl aromatic monomers. *Makromol. Chem.* **1958**, *28* (1), 253−261.
(44) Bongiovanni, R.; Sangermano, M.; Malucelli, G.; Priola, A.; Leonardi, A.; Ameduri, B.; Pollicino, A.; Recca, A. Fluorinated vinyl

https://doi.org/10.1021/acs.macromol.5c01607
Macromolecules 2025, 58, 9402−9411

ethers as new surface agents in the photocationic polymerization of vinyl ether resins. *J. Polym. Sci., Part A: Polym. Chem.* **2003**, *41* (18), 2890−2897.
(45) Discekici, E. H.; Anastasaki, A.; Kaminker, R.; Willenbacher, J.; Truong, N. P.; Fleischmann, C.; Oschmann, B.; Lunn, D. J.; Read de Alaniz, J.; Davis, T. P.; Bates, C. M.; Hawker, C. J. Light-Mediated Atom Transfer Radical Polymerization of Semi-Fluorinated (Meth)-acrylates: Facile Access to Functional Materials. *J. Am. Chem. Soc.* **2017**, *139* (16), 5939−5945.
(46) Li, D.; Yu, L.; Ning, S.; Li, P.; Chen, C.; Zhao, D.; Liao, M.; Meng, Q.; Zhang, S.; Fang, Q.; Kang, H.; Li, L.; Yang, J. Upcycling of Waste Fluororubber to Photocurable High-Performance Vinyl-Terminated Liquid Fluororubber by Multifield Coupling One-Pot Stepwise Reactions. *Adv. Sci.* **2025**, No. e01460.
(47) Luo, Y.; Luo, Y.; Qu, J.; Hou, Z. QM/MM Studies on Scandium-Catalyzed Syndiospecific Copolymerization of Styrene and Ethylene. *Organometallics* **2011**, *30* (11), 2908−2919.

https://doi.org/10.1021/acs.macromol.5c01607
Macromolecules 2025, 58, 9402−9411